

INITIAL ORBITS OF LEO OBJECTS USING RADAR OBSERVATIONS

H. Ma

RHEA System GmbH @ ESA Space Debris Office, ESA/ESOC, Robert-Bosch-Strasse 5, DE-64293 Darmstadt, Germany,
Email: helene.ma@esa.int

ABSTRACT

The space environment around Earth is being continuously exposed to risks of on-orbit break-up events and to the growing number of smaller satellites and large constellations, leading to the unavoidable growth of space debris population. Surveillance and tracking of this population including the operational satellites remain essential to monitor the space environment evolution and to protect the operational satellites, and population and infrastructure on the ground. That drives the need to develop and improve the algorithms in orbit computation.

The *Infinitesimal Angles Method* introduced in [1] is conceived to compute initial orbits of Low Earth satellites from radar data by applying a correction to the line of sight. Here a description of the extended algorithm [2] is provided, with some numerical tests to show how this method can correct the errors in the angular measurements for some simulated objects.

Keywords: Initial Orbit Determination; LEO Satellites; Earth Oblateness.

1. INTRODUCTION

Since the last decade, we observe that the population density in space environment around the Earth, in particular at low altitudes (LEO), continues to increase significantly. With the proliferation of smaller payloads accompanied by larger constellations, almost 14000 objects orbiting the Earth in LEO region were recorded in 2019 [3]. It is clear from the outset that surveillance and tracking of satellites are even more challenging nowadays. Therefore, we need to develop new methods for orbit computation and improve the existing ones. When these algorithms imply iterative calculations, it is also important to start with a good initial guess of the orbit.

A new method to compute initial orbits of LEO satellites with radar observations was introduced in [1]. Named *Infinitesimal Angles Method*, it has been extended in [2] to take into account the Earth's oblateness effect. In this paper, an overview of this technique is provided, considering the secular effect of the J_2 term of the geopotential

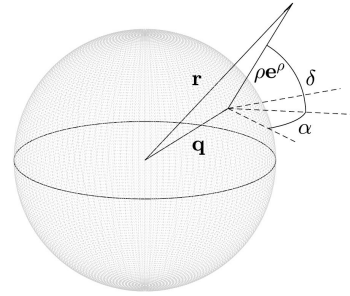


Figure 1. Geometry of the observations.

in the dynamical model. We also include some numerical tests that show the capability of this method to correct the errors in the angular measurements, and compare it with the same method but without perturbations [1].

2. ORBIT COMPUTATION WITH RADAR OBSERVATIONS

A single radar observation gives the topocentric position of the satellite at epoch t defined by $(t, \rho, \alpha, \delta)$, where ρ, α, δ are respectively the range, the right ascension and the declination. Using α and δ as angular coordinates in an equatorial reference frame (e.g. J2000), we can express the line of sight by the following unit vector

$$\mathbf{e}^\rho = (\cos \delta \cos \alpha, \cos \delta \sin \alpha, \sin \delta)^T, \quad (1)$$

and the geocentric position of the observer by \mathbf{q} . Then, the geocentric position of the observed satellite is defined by (see Fig. 1)

$$\mathbf{r} = \mathbf{q} + \rho \mathbf{e}^\rho. \quad (2)$$

We introduce the unit vectors

$$\begin{aligned} \mathbf{e}^\alpha &= (-\sin \alpha, \cos \alpha, 0)^T, \\ \mathbf{e}^\delta &= (-\sin \delta \cos \alpha, -\sin \delta \sin \alpha, \cos \delta)^T \end{aligned}$$

and the orthonormal basis $\{\mathbf{e}^\rho, \mathbf{e}^\alpha, \mathbf{e}^\delta\}$. In this basis, we can write the *geocentric* velocity of the satellite as

$$\dot{\mathbf{r}} = \xi \mathbf{e}^\alpha + \zeta \mathbf{e}^\delta + (\dot{\rho} \mathbf{e}^\rho + \dot{\mathbf{q}}) \quad (3)$$

where

$$\xi = \rho \dot{\alpha} \cos \delta, \quad \zeta = \rho \dot{\delta}, \quad (4)$$

are the components of the *topocentric* velocity of the satellite orthogonal to the line of sight, with $\dot{\alpha}, \dot{\delta}$ the angular velocities, $\dot{\rho}$ the range rate, and $\dot{\mathbf{q}}$ the observer geocentric velocity.

A *radar tracklet* is made by a set of $m \geq 4$ radar observations, which are collected at short time intervals during the same pass of the satellite. In that case, the range ρ is accurate and the line-of-sight direction given by α, δ is poorly determined.

From one tracklet we can derive the vector

$$(\bar{t}, \bar{\alpha}, \bar{\delta}, \rho, \dot{\rho}), \quad (5)$$

where \bar{t} is the mean epoch of the m observations. The quantities $\bar{\alpha}, \bar{\delta}$ are the mean values of the angles, and the values of the range ρ and the range rate $\dot{\rho}$ can be obtained by a polynomial fit. In order to compute an orbit, we have to determine the values of the angular velocities ($\dot{\alpha}, \dot{\delta}$) and provide corrections to the angles. Let us denote by $\Delta\alpha, \Delta\delta$ the unknown small deviations from $\bar{\alpha}, \bar{\delta}$ that we call the *infinitesimal angles*.

3. INFINITESIMAL ANGLES METHOD

In [1] we introduced the “*Infinitesimal Angles Method*”, an initial orbit determination (IOD) method for LEO satellites based on radar observations and assuming a pure Keplerian dynamical model [1]. This method tries to link two tracklets¹, assuming that both belong to the same object, by solving a system of eight equations in the eight unknowns $(\Delta\alpha_i, \Delta\delta_i, \dot{\alpha}_i, \dot{\delta}_i), i = 1, 2$, where the subscripts refer to the mean epochs of the tracklets, which are denoted by \bar{t}_1, \bar{t}_2 after correcting for aberration.

In [2], this method has been modified by considering in the dynamical model the secular effect of the J_2 term of the geopotential. The rates of the orbital elements due to this secular effect are given by (see [5])

$$\begin{cases} \dot{a} = 0, \\ \dot{e} = 0, \\ \dot{I} = 0, \\ \dot{\Omega} = -\frac{3}{2} J_2 \frac{R_{\oplus}^2}{p^2} \tilde{n} \cos I, \\ \dot{\omega} = \frac{3}{4} J_2 \frac{R_{\oplus}^2}{p^2} \tilde{n} (4 - 5 \sin^2 I), \\ \dot{\ell} = \tilde{n} = n \left[1 + \frac{3}{2} J_2 \frac{R_{\oplus}^2}{p^2} \left(1 - \frac{3}{2} \sin^2 I \right) \sqrt{1 - e^2} \right], \end{cases} \quad (6)$$

where $p = a(1 - e^2)$ is the parameter of the two-body trajectory and $n = \sqrt{\mu/a^3}$ the mean motion. We note

¹Note that we use the term *radar track* in [1] and [2], which has the same meaning as *radar tracklet* in this paper.

that only the right ascension of the ascending node Ω , the argument of perigee ω , and the mean anomaly ℓ change uniformly with time, while the other orbital elements remain constant.

Equations (6) can shortly be written as

$$\dot{\mathcal{E}}_{kep} = \mathbf{X}_{kep}(\mathcal{E}_{kep}), \quad (7)$$

with the Keplerian coordinates $\mathcal{E}_{kep} = (a, e, I, \Omega, \omega, \ell)$ for the orbits. In the following, we shall assume that the observed satellite moves according to the dynamics defined by Equations (6), (7).

3.1. Projections of the equations of motion

We want to write the equations of motion (6) in Cartesian coordinates $\mathcal{E}_{car} = (\mathbf{r}, \dot{\mathbf{r}})$. To do so, we first convert Equation (7) in

$$\dot{\mathcal{E}}_{car} = \mathbf{Y}(\mathcal{E}_{car}) \quad (8)$$

where

$$\mathbf{Y} = \left(\frac{\partial \phi_1}{\partial \mathcal{E}_{kep}} \mathbf{X}_{kep} \right) \circ \phi_1^{-1}$$

is the transformed vector field with the coordinate change

$\mathcal{E}_{kep} \xrightarrow{\phi_1} \mathcal{E}_{car}$. Then, from the expression above we get the acceleration $\ddot{\mathbf{r}}$ as a function of \mathcal{E}_{car} along the solutions of (8):

$$\ddot{\mathbf{r}} = \left(\frac{\partial \dot{\mathbf{r}}}{\partial \mathcal{E}_{kep}} \mathbf{X}_{kep} \right) \circ \phi_1^{-1} =: \tilde{\mathbf{y}}(\mathbf{r}, \dot{\mathbf{r}}). \quad (9)$$

The equations of motion (9) are projected along the line of sight \mathbf{e}^o at each epoch $t_i, i = 1, 2$, thus obtaining two equations of the form

$$\begin{aligned} \mathcal{K} &= 0 \\ &= (\ddot{\mathbf{r}} - \tilde{\mathbf{y}}) \cdot \mathbf{e}^o \\ &= \ddot{\rho} - \rho \eta^2 + \ddot{\mathbf{q}} \cdot \mathbf{e}^o - \tilde{\mathbf{y}} \cdot \mathbf{e}^o. \end{aligned} \quad (10)$$

The quantity $\eta = \sqrt{\dot{\alpha}^2 \cos^2 \delta + \dot{\delta}^2}$ is the *proper motion*.

3.2. The evolution of the two-body integrals

We recall the first integrals of Kepler’s problem: the angular momentum \mathbf{c} , the energy \mathcal{E} , and the Laplace-Lenz vector \mathbf{L} . They are expressed as functions of $\mathbf{r}, \dot{\mathbf{r}}$ as follows:

$$\begin{aligned} \mathbf{c} &= \mathbf{r} \times \dot{\mathbf{r}}, \\ \mathcal{E} &= \frac{1}{2} |\dot{\mathbf{r}}|^2 - \frac{\mu}{|\mathbf{r}|}, \\ \mathbf{L} &= \frac{1}{\mu} \dot{\mathbf{r}} \times \mathbf{c} - \frac{\mathbf{r}}{|\mathbf{r}|}. \end{aligned}$$

Between the epochs \tilde{t}_1, \tilde{t}_2 of the tracklets, the angular momentum and the Laplace-Lenz vector are not conserved anymore if the J_2 perturbation is included. In fact, assuming the secular J_2 model (6), the following relations hold (see Fig. 2):

$$\begin{aligned} R_c \mathbf{c}_1 &= \mathbf{c}_2, \\ \mathcal{E}_1 &= \mathcal{E}_2, \\ R_L \mathbf{L}_1 &= \mathbf{L}_2, \end{aligned} \quad (11)$$

where

$$R_c = R_{\Delta\Omega}^{\hat{\mathbf{z}}}, \quad R_L = R_{\omega_1 + \Delta\omega}^{\hat{\mathbf{c}}_2} R_{\Delta\Omega}^{\hat{\mathbf{z}}} R_{-\omega_1}^{\hat{\mathbf{c}}_1}.$$

Here $R_{\varphi}^{\mathbf{v}}$ denotes the rotation of an angle φ around the axis defined by vector \mathbf{v} . The unit vectors $\hat{\mathbf{z}}, \hat{\mathbf{c}}_i, i = 1, 2$, are defined as

$$\begin{aligned} \hat{\mathbf{z}} &= (0, 0, 1)^T, \\ \hat{\mathbf{c}}_i &= (\sin \Omega_i \sin I_i, -\cos \Omega_i \sin I_i, \cos I_i)^T. \end{aligned}$$

Using Equations (6), the angular variations $\Delta\Omega$ and $\Delta\omega$ can be determined by the formulae:

$$\Delta\Omega = \dot{\Omega}_1(\tilde{t}_2 - \tilde{t}_1), \quad \Delta\omega = \dot{\omega}_1(\tilde{t}_2 - \tilde{t}_1). \quad (12)$$

Note that Equations 12 can also be written by $\Delta\Omega = \Omega_2 - \Omega_1, \Delta\omega = \omega_2 - \omega_1$.

Let us define the vector $\mathbf{v}_2 = \mathbf{e}_2^{\rho} \times \mathbf{q}_2$. The relation involving the Laplace-Lenz vectors (see the last equation in 11) is projected onto \mathbf{v}_2 . Finally, the evolution of the two-body integrals is given by:

$$\begin{aligned} R_c \mathbf{c}_1 - \mathbf{c}_2 &= \mathbf{0}, \\ \mathcal{E}_1 - \mathcal{E}_2 &= 0, \\ (R_L \mathbf{L}_1 - \mathbf{L}_2) \cdot \mathbf{v}_2 &= 0. \end{aligned} \quad (13)$$

3.3. Lambert's equation under J_2 effect

Given a pure elliptic motion, Lambert's theorem states that the orbital transfer time $t_2 - t_1$ only depends on the semi-major axis a , the sum $r_1 + r_2$ of the two distances $r_1 = |P_1 - F|, r_2 = |P_2 - F|$ from the centre of force F , and the length d_L of the chord joining the two positions [1, 6].

We can apply this theorem to the two geocentric positions $\mathbf{r}_1, \mathbf{r}_2$ of an observed object at epochs \tilde{t}_1, \tilde{t}_2 . In the dynamics given by (6), the mean motion evolves linearly with time. If we denote the expression defining Lambert's equation by \mathcal{L} , we have

$$\mathcal{L} = \tilde{n}(\tilde{t}_1 - \tilde{t}_2) + (\beta - \sin \beta) - (\gamma - \sin \gamma) + 2k\pi = 0, \quad (14)$$

where \tilde{n} is taken from the last equation in (6), and $k \in \mathbb{N}$ is the number of revolutions in the interval $[\tilde{t}_1, \tilde{t}_2]$.

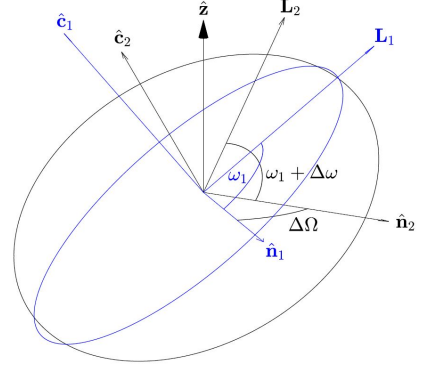


Figure 2. According to the secular J_2 model (6), the shape of the orbit and its inclination remain unchanged between two epochs \tilde{t}_1, \tilde{t}_2 . The directions of the angular momentum ($\hat{\mathbf{c}}$), line of nodes ($\hat{\mathbf{n}}$) (see 16) and Laplace-Lenz vector (\mathbf{L}), by contrast, are rotated due to the secular variations $\Delta\Omega, \Delta\omega$ accumulated during the time interval $\tilde{t}_2 - \tilde{t}_1$.

The angles β, γ are defined by

$$\sin^2 \frac{\beta}{2} = \frac{r_1 + r_2 + d_L}{4a}, \quad \sin^2 \frac{\gamma}{2} = \frac{r_1 + r_2 - d_L}{4a}, \quad (15)$$

where $0 \leq \beta - \gamma \leq 2\pi$ and $r_1 = |\mathbf{r}_1|, r_2 = |\mathbf{r}_2|$ are the two geocentric distances of the observed object at epochs \tilde{t}_1, \tilde{t}_2 .

In (15) the length of the chord

$$d_L = |\tilde{R}\mathbf{r}_1 - \mathbf{r}_2|$$

is obtained after rotating the osculating ellipse at \tilde{t}_1 so that it overlaps with the osculating ellipse at \tilde{t}_2 . Precisely, the position \mathbf{r}_1 is subject to the rotation \tilde{R} , which is explicitly given by

$$\tilde{R} = \tilde{R}_2 \tilde{R}_1^T,$$

with

$$\tilde{R}_1 = R_{\omega_1}^{\hat{\mathbf{c}}_1} R_{I_1}^{\hat{\mathbf{n}}_1} R_{\Omega_1}^{\hat{\mathbf{z}}}, \quad \tilde{R}_2 = R_{\omega_1 + \Delta\omega}^{\hat{\mathbf{c}}_2} R_{I_2}^{\hat{\mathbf{n}}_2} R_{\Omega_1 + \Delta\Omega}^{\hat{\mathbf{z}}},$$

and where

$$\hat{\mathbf{n}}_i = (\cos \Omega_i, \sin \Omega_i, 0)^T, \quad i = 1, 2, \quad (16)$$

are the directions of the lines of nodes. In fact, \tilde{R}_1 and \tilde{R}_2 represent the transformations from the selected equatorial reference frame to the orbital reference frame at the epochs \tilde{t}_1 and \tilde{t}_2 , respectively.

3.4. Solving a linkage problem

The *Infinitesimal Angles Method* tries to join the data from two radar tracklets of the form (5), to compute one

or more initial orbits. The subscripts 1, 2 are used to distinguish the quantities according to the epochs of the two tracklets.

The system to be solved is made by the eight equations

$$(R_c \mathbf{c}_1 - \mathbf{c}_2, \mathcal{E}_1 - \mathcal{E}_2, \mathcal{K}_1, \mathcal{K}_2, (R_L \mathbf{L}_1 - \mathbf{L}_2) \cdot \mathbf{v}_2, \mathcal{L}) = \mathbf{0} \quad (17)$$

in the eight unknowns

$$\mathbf{X} = (\xi_1, \zeta_1, \xi_2, \zeta_2), \quad \Delta = (\Delta\alpha_1, \Delta\delta_1, \Delta\alpha_2, \Delta\delta_2), \quad (18)$$

where Δ is the vector of the infinitesimal angles.

To solve system (17), we split it into the two subsystems

$$\mathcal{G}(\Delta) = \mathbf{G}(\mathbf{X}(\Delta), \Delta) = \mathbf{0}, \quad (19)$$

$$\mathcal{J}(\mathbf{X}) = \mathbf{J}(\mathbf{X}, \Delta) = \mathbf{0}, \quad (20)$$

where

$$\begin{aligned} \mathbf{G} &= (\mathcal{K}_1, \mathcal{K}_2, (R_L \mathbf{L}_1 - \mathbf{L}_2) \cdot \mathbf{v}_2, \mathcal{L}), \\ \mathbf{J} &= (R_c \mathbf{c}_1 - \mathbf{c}_2, \mathcal{E}_1 - \mathcal{E}_2). \end{aligned}$$

A double-iteration scheme is used to solve the subsystems, consisting of two nested Newton-Raphson methods. The Newton-Raphson method at the outer loop of the scheme computes the vector Δ from subsystem (19) using the iterative formula

$$\Delta_{h+1} = \Delta_h - \left[\frac{\partial \mathcal{G}}{\partial \Delta}(\Delta_h) \right]^{-1} \mathcal{G}(\Delta_h) \quad (21)$$

with the Jacobian matrix $\frac{\partial \mathcal{G}}{\partial \Delta}$ of the subsystem (19).

Given $\Delta = \Delta_h$ at the h -th iteration, the inner Newton-Raphson method is applied to compute $\mathbf{X}^{(h)} = \mathbf{X}(\Delta_h)$ from subsystem (20) using the iterative formula

$$\mathbf{X}_{j+1} = \mathbf{X}_j - \left[\frac{\partial \mathcal{J}}{\partial \mathbf{X}}(\mathbf{X}_j) \right]^{-1} \mathcal{J}(\mathbf{X}_j) \quad (22)$$

with the Jacobian matrix $\frac{\partial \mathcal{J}}{\partial \mathbf{X}}$ of the subsystem (20).

3.5. At iteration $h = 0$

Let (\mathbf{X}_0, Δ_0) be the starting guess of the double-iterative scheme. At $h = 0$, the vector \mathbf{X}_0 is computed from the interpolated values of $\delta, \dot{\alpha}, \dot{\delta}, \rho$ through the expressions in (4). The vector Δ_0 can be set equal to $\mathbf{0}$, taking advantage of the assumed smallness of the angle deviations.

The vector $\mathbf{X}^{(0)}$ such that $\mathbf{J}(\mathbf{X}^{(0)}, \Delta_0) = \mathbf{0}$ is calculated through formula (22). At this stage the number of revolutions k is also computed as it is required in subsystem (19) for Lambert's equation. It is obtained by

$$k = \left\lfloor \frac{n(\tilde{t}_2 - \tilde{t}_1)}{2\pi} \right\rfloor$$

where n is the mean motion, $\lfloor x \rfloor$ denotes the integer part of x . We perform the first iteration of the outer Newton-Raphson method with the formula (21) wherein $\mathcal{G}(\Delta_0) = \mathbf{G}(\mathbf{X}^{(0)}, \Delta_0)$.

Table 1. Keplerian elements at epochs $\tilde{t}_1 = 54127.1553819$ MJD and $\tilde{t}_2 = 54127.2991319$ MJD for Object 1 and Object 2, respectively. The values of a, e, I are exact, the others are approximated. Distances are in km, angles in degrees [2].

Object	1	2
a	7818.10	7396.00
e	0.0658	0.0341
I	65.81	26.88
Ω	213.92	255.49
ω	356.70	357.13
ℓ	202.25	198.67

3.6. At iteration $h \geq 1$

For the following iterations of the double-iterative scheme, we set $\mathbf{X}_0 = \mathbf{X}^{(h-1)}$ as the updated starting guess of vector \mathbf{X} , and the iterations continue until we reach a suitable tolerance on the magnitude of the difference $\Delta_h - \Delta_{h-1}$. Once the convergence has been attained, we compute the vector $\mathbf{X}^{(h)}$ with (22) to obtain the solution(s) $(\mathbf{X}^{(h)}, \Delta_h)$ of the system (17).

All the derivatives involved in the double-iterative scheme can be found in [1] and [2].

4. EXAMPLES OF NUMERICAL TESTS

We extract here two examples of numerical tests using simulated data from [2]. Let us consider two objects whose orbital elements at their respective epoch \tilde{t}_1 are defined in Tab. 1. Note that for the selected orbits, the J_2 perturbation is the dominant one if a small area-to-mass ratio of the two objects is assumed [7], and the J_2 effect will be stronger for Object 2 as the inclination and semi-major axis are smaller.

We use a two-body propagation with the secular effect of J_2 (Equations in 6) in order to generate two radar tracklets for each object. Each tracklet is composed of four observations taken at time intervals of 10 s. The tracklets for Object 1 are separated by $k = 13$ revolutions, while those for Object 2 are separated by $k = 8$ revolutions.

We add to ρ, α, δ a Gaussian error with zero mean and different standard deviations (RMS) shown in Tab. 2. The interpolated data that are obtained after adding the noise to the simulated observations are given in Tab. 3, 4 for Objects 1, 2, respectively.

The absolute differences between the computed orbital elements and the *true* ones (see Tab. 1) of Objects 1, 2 are shown in Tab. 5. We show the results for the method including the J_2 effect (IA- J_2) and the method that con-

Table 2. Standard deviation (RMS) of the errors added to ρ , α , δ of the radar tracklets. These levels of noise correspond to the Cases 3 and 4 in [2].

	α, δ ($^\circ$)	ρ (m)
Case 1	0.15	1
Case 2	0.15	10

siders a pure Keplerian motion (IAQ) described in [1], with the noise levels of Tab. 2.

The method IAQ does not find a good orbit for Object 1 with the tracklets separated by 13 revolutions, while we can be satisfied to see how IA- J_2 is able to correct the errors in the angles α , δ and to recover the known orbits for both objects. We can observe that with a higher noise level in ρ (Case 2), the performance of the method IA- J_2 is slightly worse for the eccentricity of Object 1, while it is almost unchanged for the orbital elements of Object 2. Tab. 6 shows the corrections provided by the method IA- J_2 to the angles α, δ for both objects.

5. CONCLUSION

The J_2 effect was included in the dynamical model of the *Infinitesimal Angles method* that computes initial orbits of LEO satellites using radar data. This method attempts to perform a linkage of two radar tracklets by solving the system (17) in the unknowns (18) using a double-iterative scheme.

The numerical tests with simulated data show the ability of this algorithm to correct the errors in the angles α , δ and to recover the Keplerian elements of the known orbit. An overview of this method is provided in this paper, and details and complementary numerical tests can be found in [1] and [2].

Possible future developments of this work consist in comparing the method with other existing IOD methods such as in [4], also taking large datasets of real observations, and the inclusion in the dynamical model of the perturbation represented by the atmospheric drag.

ACKNOWLEDGMENTS

The author would like to thank G. F. Gronchi, D. Bracali Cioci, and in particular G. Baù for reviewing this paper and for recommending useful suggestions. This work was partially supported by the Marie Curie Initial Training Network Stardust, FP7-PEOPLE-2012-ITN, Grant Agreement 317185.

REFERENCES

1. Gronchi G. F., Dimare L., Bracali Cioci D., Ma H., (2015). On the computation of preliminary orbits for Earth satellites with radar observation, *Monthly Notices of the Royal Astronomical Society*, **451**, 2, pp. 1883-1891.
2. Ma H., Baù G., Bracali Cioci D., Gronchi G. F., (2018). Preliminary orbits with line-of-sight correction for LEO satellites observed with radar, *Celestial Mechanics and Dynamical Astronomy*, **130**, 70.
3. ESA Space Debris Office., (2020). ESA's Annual Space Environment Report, version 4.0. Online at https://www.sdo.esoc.esa.int/environment_report/Space_Environment_Report_latest.pdf.
4. Farnocchia D., Tommei G., Milani A., Rossi A., (2010). Innovative methods of correlation and orbit determination for space debris, *Celestial Mechanics and Dynamical Astronomy*, **107**, 1-2, pp.169-185.
5. Roy A. E., (2004). Orbital Motion, *CRC Press*, Edition 4.
6. Battin R. H., (1999). An Introduction to the Mathematics and Methods of Astrodynamics, *AIAA Education Series*, AIAA, Reston, VA, Revised Edition.
7. Montenbruck O., Gill E., (2000). Satellite Orbits - Models, Methods and Applications, *Springer*, The Netherlands, First Edition.

Table 3. Data interpolated from the radar tracklets of Object 1 at epochs $\bar{t}_1 = 54127.5824653$ MJD and $\bar{t}_2 = 54128.6241320$ MJD, using the two different noise levels of Tab. 2 [2].

Epoch	Case	$\bar{\alpha}$ (°)	$\bar{\delta}$ (°)	$\dot{\alpha}$ (°/s)	$\dot{\delta}$ (°/s)	ρ (km)	$\dot{\rho}$ (km/s)
Object 1, $k = 13$							
\bar{t}_1	1	242.95755	-79.11215	-0.01356	0.16825	1875.98971	-4.84829
	2	242.95755	-79.11215	-0.01356	0.16825	1875.98562	4.84735
\bar{t}_2	1	204.34455	53.03103	0.11860	0.10845	2061.14383	5.59005
	2	204.34455	53.03103	0.11860	0.10845	2061.15395	5.58735

Table 4. Data interpolated from the radar tracks of Object 2 at epochs $\bar{t}_1 = 54127.6906251$ MJD and $\bar{t}_2 = 54128.3300348$ MJD, using the two different noise levels of Tab. 2 [2].

Epoch	Case	$\bar{\alpha}$ (°)	$\bar{\delta}$ (°)	$\dot{\alpha}$ (°/s)	$\dot{\delta}$ (°/s)	ρ (km)	$\dot{\rho}$ (km/s)
Object 2, $k = 8$							
\bar{t}_1	1	162.41862	-0.70695	0.12744	0.07974	1914.59715	-5.09806
	2	162.41862	-0.70695	0.12744	0.07974	1914.59305	-5.09712
\bar{t}_2	1	169.53245	-20.90422	0.14196	-0.01396	2013.14698	4.73488
	2	169.53245	-20.90422	0.14196	-0.01396	2013.15710	4.73218

Table 5. Absolute errors in the orbital elements of Objects 1, 2 at epoch \bar{t}_1 for the noise levels of Tab. 2 [2]. Note that IAQ does not work with Object 2.

	Object 1, $k = 13$		Object 2, $k = 8$	Case
	IAQ	IA- J_2	IA- J_2	
δa	502.4785	0.0105	0.1615	1
	502.4096	0.0116	0.1378	2
δe	4.32×10^{-3}	7.08×10^{-5}	2.00×10^{-4}	1
	4.76×10^{-3}	1.44×10^{-4}	1.50×10^{-4}	2
δI	6.2022	0.0977	0.9485	1
	6.2071	0.0830	0.6724	2
$\delta \Omega$	5.1509	0.0469	0.5746	1
	5.1487	0.0454	0.3900	2
$\delta \omega$	129.2975	0.0203	4.7886	1
	129.3858	0.0388	3.5505	2
$\delta \ell$	239.9665	0.0124	4.2105	1
	239.8206	0.0095	3.1483	2

Table 6. Infinitesimal angles in degrees found by the method IA- J_2 using the radar tracklets of Tab. 3 and 4 for Objects 1 and 2 respectively [2].

	Object 1, $k = 13$		Object 2, $k = 8$	
	Case 1	Case 2	Case 1	Case 2
$\Delta \alpha_1$	0.25737	0.08057	-0.01612	-0.00648
$\Delta \delta_1$	0.08058	0.07575	-1.54546	-1.12770
$\Delta \alpha_2$	-0.23547	-0.24423	0.03328	0.00800
$\Delta \delta_2$	-0.02666	-0.04653	-3.45550	-2.44161